Development and Design of Elastic, Rubber-based Mounts for Different Components of Windmills: Example and Engineering Backgrounds

Thomas Böhme*[,a], Alexander Padios[a], Stefan Wolter[a]

Freudenberg Schwab Vibration Control, Berliner Str. 17, 16727 Velten, Germany

Abstract

The present contribution illustrates different aspects of designing and calculation of vibration control components within windmills. The necessity for vibration control and acoustics is motivated and different, widely used design solutions are presented. Typical engineering approaches are explained that allows to develop rubber-based, elastic components. Furthermore questions of rubber life-time are discussed and in-field experiments w.r.t. dynamical analysis of power generation components are illustrated.

Keywords

rubber, vibration control, power-train, elastic mounts, decoupling, insulation, damping, durability, life-time

1. Introduction

Vibrations and noise represent an important technical topic for modern windmills. Legal requirements, ecological aspects or technical issues such as durability require a detailed estimation, evaluation and partially reduction of occurring excitations and vibrations, e. g. along the power train. For this reason so-called Rubber-To-Metal parts (RTMs) are widely used in windmills. In particular, elastomeric couplings and rubber-based mountings can be found along the power train – especially within so-called non-direct windmills, i.e. windmills with gear-box - in order to decouple different excitations and to reduce vibrations and sound emissions. By considering non-direct windmills RTMs can be classified as follows, cf., Figure 1:

a. **Control box mountings:** control units contain various, sensitive electrical devices, which may fail under the continuous appearance of vibrations or singular impacts (e.g. in case of emergency stop). For this reason elastic mounts are used to decouple such components, e.g. pitch control units, from the exciting structure.

b. **Couplings:** Elastomeric couplings are used along the power train in order to correct spatial displacements, which follow from manufacturing tolerances or thermal expansion. Such displacements would result in constraint forces, which may cause accelerated failure of power train components. Furthermore couplings reduce and damp the amplitudes of torque shocks and reduce the transmission of structure borne noise. For a detailed explanation we refer to the corresponding DIN Standard, [1].

c. **Gear box mountings:** Obviously these components are only relevant for non-direct windmills and act as a torque support. Such mounts are confronted with the following trade-off: On the one hand side considerable torques and torques variations must be stabilized in order to minimize rolling of the gear box. For this reason stiff mountings are preferred. On the other hand gear boxes generates noises, caused by the meshing of the gears. These noises have a pronounced tonality and could be amplified by large surfaces (e.g. tower or blades), [2,4]. Here smooth mounts would be advantageous. Therefore a technical compromise must be found or hydraulic mountings must be assembled, which show a smooth stiffness for vertical, translational deflections and stiff behaviour for rotations around the power train, [3] and Figure 2.

d. **Generator mountings:** A separate generator is typically found in non-direct windmills, whereas in direct plants the electromagnetic coils are usually fixed directly at the circular nacelle cover. Here elastic mountings remedy the transfer of loads or deformations into the power train following from

* Author for correspondence (thomas.boehme@schwab-vc.com).

[a] Present address: Berliner Str. 17, 16727 Velten, Germany

deformations of the windmill structure (e.g. due to temperature changes). Furthermore elastic connections prevent the transfer of structure borne noise and insulate the generator w.r.t. torsional vibrations of the shaft, which result from aero-dynamical excitations or electrical system perturbation.

e. **Cooling package mounts:** These components are used for a consequent sound optimization. Especially any periodic movements (here movements of the fan) and eventually resulting vibration transmission to the structure, which – in turn – may cause sound emission via large surfaces should be minimized.

f. **Mounts for nacelle cover**: In principle, there are two different strategies for decouple structure borne noise: **(i)** active vibration insulation, i.e. elastic mounting at the vibration source (exciting component), or **(ii)** passive insulation, i.e. elastic mounting of the units, which have to be protected. Passive insulation is recommended in case of unknown or multiple vibration sources. The nacelle cover represents a thin-wall, large surface, which could act as a sound amplifier and transmitter and – consequently – should be passively insulated.

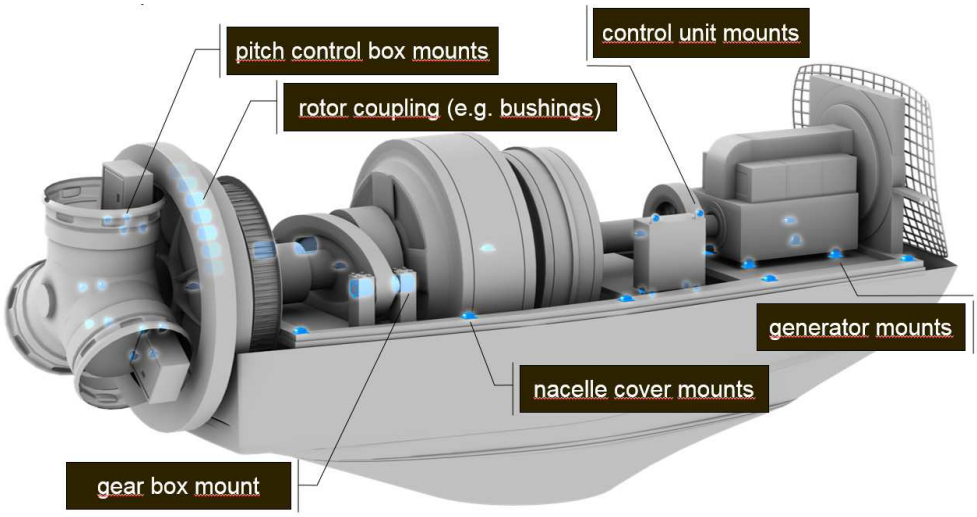

Figure 1: Various rubber-to-metal components within a non-direct windmill.

Please note, the materials behaviour of rubber significantly differs to metals and consequently many engineers feel unsure during designing and calculation of RTMs, especially under the impression of the occurring, considerable loads. For this reason the present article will illustrate, how RTMs are designed by taking into account questions of required insulation, strengths or sufficient life-time of used materials.

2. Design and Calculation of Rubber-To-Metal Components

2.1 Fundamentals of Vibrations: Transmissibility, Insulation and Damping

For simplicity reasons we restrict the following calculations to the one-dimensional auxiliary system, displayed in Figure 3 (left). The corresponding Ordinary Differential Equation (ODE) reads:

$$m\ddot{x} + b\dot{x} + cx = F_{\mathrm{ex}} \quad , \quad (y \equiv 0) \quad , \quad \text{(damped oscillation with forced excitation).} \tag{1}$$

Here F_{ex} stands for the external force acting at the elastically mounted mass. Furthermore c [N/mm] and b [Ns/mm] represent the mounting stiffness or the damping constant, respectively. Without loss of generality we assume a harmonic excitation as follows ($F_0, x_0 = F_0/c$: maximal values = amplitudes):

$$F_{\mathrm{ex}}(t) = F_0 \cos(\Omega t) \quad , \quad \text{(excitation by force)} \ . \tag{2}$$

By introducing the following important abbreviations $\omega_0 = \sqrt{c/m}$, (angular velocity); $\eta = \Omega/\omega_0$, (frequency ratio); and $2D = b/\sqrt{mc}$, (damping coefficient) allows us to modify Eq. (1) as follows:

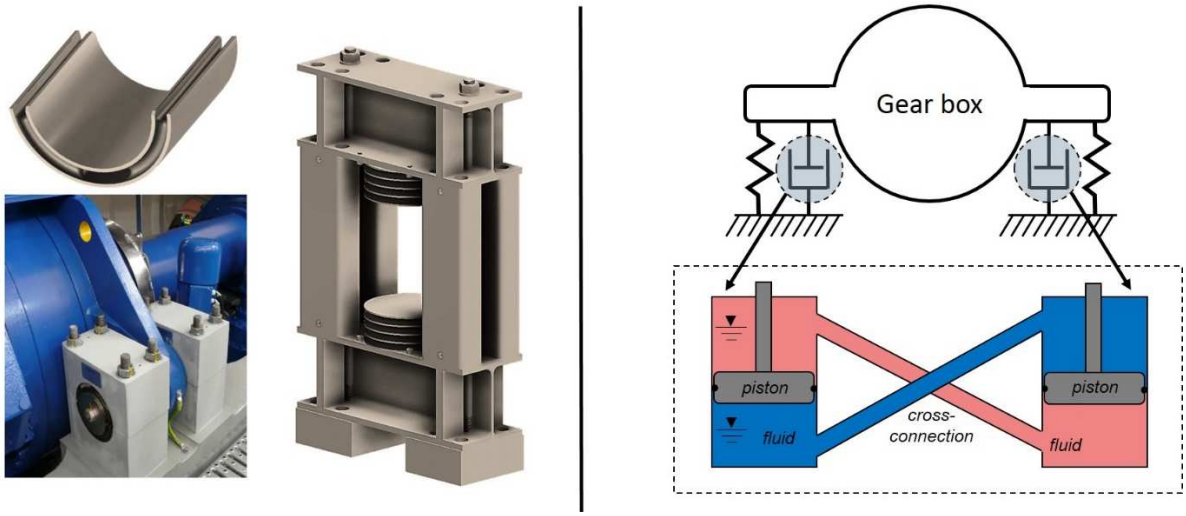

Figure 2: *Left*: half-shell or layered spring for gear box mountings. *Right*: Schematic illustration of hydraulic torque support with cross-connection of fluid chambers.

$$\ddot{x} + 2D\omega_0\dot{x} + {\omega_0}^2 x = \frac{F_0}{m}\cos(\Omega t) \tag{3}$$

with the system-specific, damped eigenfrequency f_d:

$$f_d = \frac{\omega_d}{2\pi} \quad , \quad \omega_d = \omega_0\sqrt{1-D} \quad , \quad \omega_0 = 2\pi f_0 = \sqrt{\frac{c}{m}} \ . \tag{4}$$

The solution of this inhomogeneous ODE can be found in standard literature of mechanical engineering, cf., for example [5,7]. The general solution reads:

$$x(t) = X\cos(\Omega t - \phi) \quad \text{with} \quad X = V_1\frac{F_0}{c} = V_1 x_0 \quad \text{and} \quad \tan(\phi) = \frac{2D\eta}{1-\eta^2} \ . \tag{5}$$

Here x_0 represents the displacement amplitude resulting from the excitation F_0. Furthermore ϕ stands for the angular phase shift due to damping. The quantity V_1 denotes the so-called transmissibility, which characterizes the amplitude ratio between reacting amplitude of the system and exciting amplitude, i.e. $V_1 = X/x_0$. In particular the following expression holds:

$$V_1(D,\eta) = \frac{1}{\sqrt{(1-\eta^2)^2+4D^2\eta^2}} \quad , \quad \text{(excitation by force)} \ . \tag{6}$$

For the sake of completeness we also note the transmissibility in case of velocity-dependent displacement excitation $y(t) = y_0\cos(\Omega t)$: $V_2(D,\eta) = \sqrt{1+4D^2\eta^2}/\sqrt{(1-\eta^2)^2+4D^2\eta^2} = X/y_0$.

The damping coefficient as well as the damping constant, *D* or *b*, respectively must be experimentally quantified. For this reason dynamical load-unload experiments of mounts are performed, which yield a hysteresis curve in the load-deflection diagram, see Figure 4. (right).

Please note, the underlying rheological model, cf., Figure 3 (left), represents the so-called Kelvin-Voigt model with a viscous damping element. For harmonic dynamics follows $F = cx + b\dot{x}$ with $\dot{x} = \Omega x$ or in terms of stresses $\sigma = c(1 + \Omega b/c)\varepsilon$. Moreover, in case of harmonic temporal functions for load and deflection the hysteresis represents an ellipsis, cf., Figure 4 (left). Here Young's modulus can be expressed as a complex number, $\sigma = (E' + \mathrm{i}E'')\varepsilon = E'[1 + \mathrm{i}\tan(\delta)]\varepsilon$, with the so-called loss angle [rad]: $\delta = E''/E'$, [8].

One of the most illustrative quantities for damping denotes the damping factor, $\Psi = W/U$, which represents the ratio between dissipated work and work of the corresponding linear-elastic spring, cf., Figure 4 (right). For elliptic areas holds $\Psi = 2\pi\tan(\delta)$. By comparing the coefficients of ε in the afore-mentioned expressions for σ yields the following relations, [8]:

$$\Omega b/c = \tan(\delta) \quad \Leftrightarrow \quad D = \frac{1}{2}\tan(\delta) \quad \Leftrightarrow \quad D = \frac{\Psi}{4\pi} . \tag{7}$$

Eq. (7) has important character, since the different relations connect the damping variable *D* (and consequently *b*) to experimental quantities Ψ or δ, respectively.

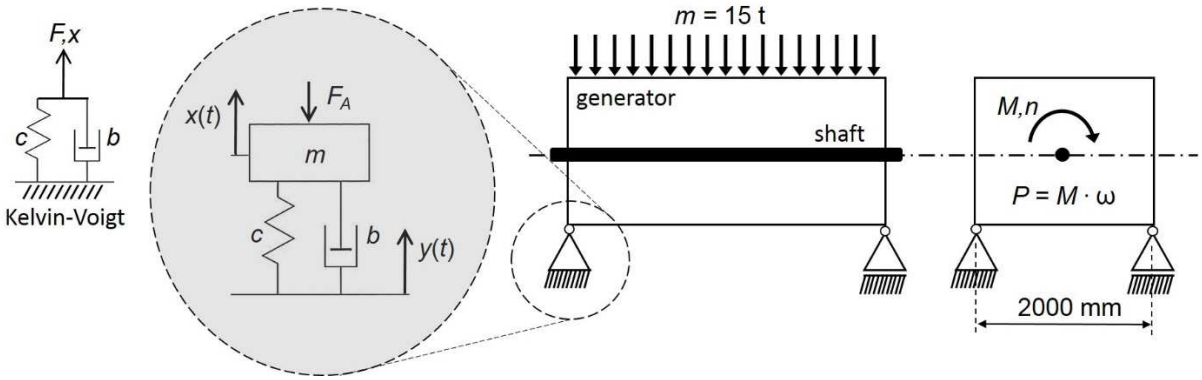

Figure 3: Schematic illustration of the mounting situation of the calculated generator.

The above framework allows to calculate vibration control components with focus on insulation and damping demands of the oscillating system. Here insulation describes the system adjustment, for which $V_{1/2} < 1$ holds. For the sake of convenience let us consider the un-damped case. Here $V_{1/2}$ only depends on the frequency ratio η. Combining Eq. (6) with Eq. $(4)_3$ and using $c = mg/\Delta z$ yields the excitation frequency as function of static deflection Δz. Figure 5 (right) shows the result in a double logarithmic scale, the so-called insulation map.

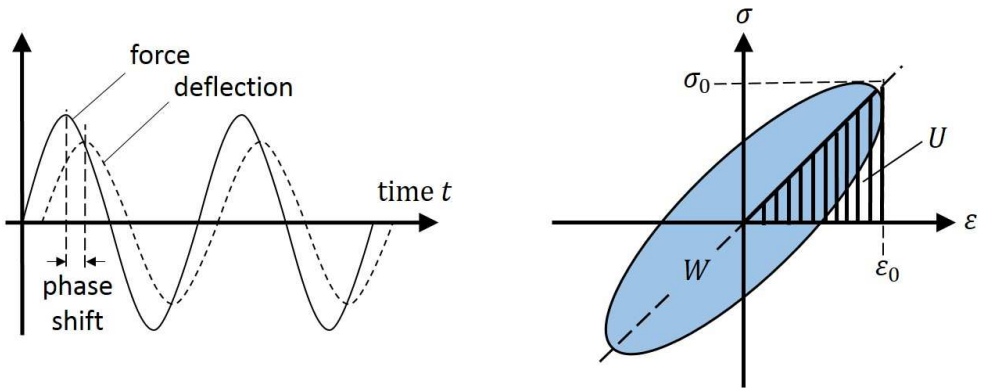

Figure 4: *Left*: Harmonic, load-unload experiment and illustration of phase shift between force and deflection due to damping. *Right*: Elliptic hysteresis and illustration of dissipated work *W*.

Let us exemplarily turn the attention to the mountings of the generator in a non-direct windmill. Basically the power train represents a complex oscillating system, consisting of different masses and springs, [9]. An isolated consideration of the generator only holds in a very limited degree.

Due to the different forms of transmissibility $V_{1/2}$ it is very important to initially clarify the nature of excitation (displacement- vs. force-controlled) as well as the target of the calculation (minimization of generator oscillations $x(t)$ vs. minimization of oscillation transmission to the flexible basis, i.e. ratio $x(t)/y(t)$). For the present example we exemplarily consider force excitations following e. g. from torque variations in the power train or from shocks (e.g. emergency stops) and ask for minimization of generator movements.

We assume the following technical data during the calculation: *m* = 15 t (weight of generator), *n* = 1500 rpm (speed), *P* = 3 MW (power). Furthermore a 4-point mounting system, a rectangular generator geometry, as illustrated in Figure 3 (right), and an ad hoc excitation frequency of f_0 = 10 Hz = 600 rpm is considered. It is worth-mentioning that higher orders of the 3P rotor excitations could coincide with f_0, [9]. In such case, the different masses of the power train, i.e. also the generator mass, start to oscillate according to the eigenmode.

Let us declare a target insulation value of 60 percent ($V_1 = 0.4$). From the insulation map we find a target static mount deflection of $\Delta z \approx 10$mm. Moreover, the resulting weight per mount denotes 3750 kg. Consequently we obtain a target mount stiffness of 3750 N/mm. Figure 5 (right) illustrates the corresponding transmissibility. Please note, beyond stationary excitation of 600 rpm transient situations occur, i.e. running-up process or emergency stop, which may cause resonance cases. In order to avoid large deflections in such events, mounts with increased damping properties could be useful. Figure 5 (left) illustrates the reduced deflections during resonance, in which the following typical values were used for the loss angle: $\delta_{\mathrm{NR}} = 3° - 5°$ and $\delta_{\mathrm{high-damp}} = 15° - 20°$.

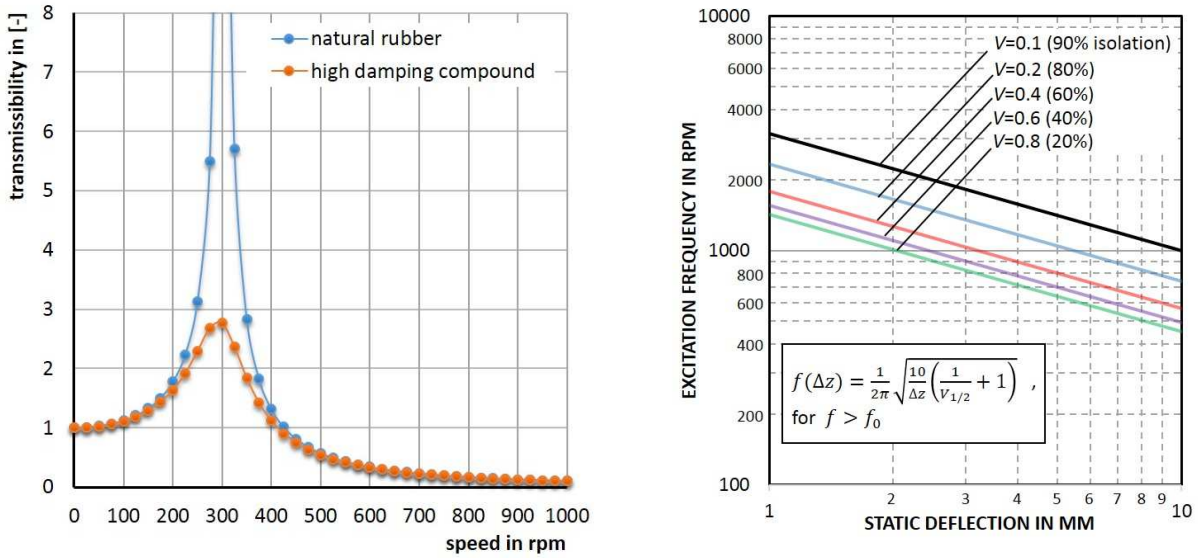

Figure 5: *Left*: transmissibility of generator mounts for different rubber compounds. *Right*: Insulation map for graphical determination of target mount stiffness (by means of deflection and defined mass).

2.2 Strength calculation of rubber

Rubber materials show a very good elastic behaviour and – additionally – inherent damping due to internal friction. With rubber failure strains, ε_f, up to 650 percent can be reached. However, comparing to steel the tensile strength and shear modulus, R_m and G, is much less, e.g. for natural rubber NR: $R_\mathrm{m} \cong 20$ MPa and $G \cong 1$ MPa. Furthermore rubber is nearly incompressible, i.e. $\nu \cong 0.5$ (Poisson's ratio). Please note, at RTM parts the rubber is chemically bonded to the metal via bonding agents. Here, during deformation, the rubber have to spread via free surfaces due to its incompressibility. If there is no free surface, the rubber would not be deformable, consequently the ratio between bonded and free surface, represented by the form factor q, have a crucial influence on the stiffness of the RTM part.

2.2.1 Stiffness

In contrast to the material specific shear modulus and due to above mentioned existence of bonded surfaces Young's modulus, E, is strongly affected by the geometry of the RTM part. For illustrative reasons we consider in the following explanations the simple geometry of circular mounts, cf., Figure 6. This example can also be used to calculate layered springs, cf., Figure 2 (left) or, with some limitations, bushings. For complex geometries a Finite Element Analysis (FEA) must be performed, cf., Section 2.2.2.

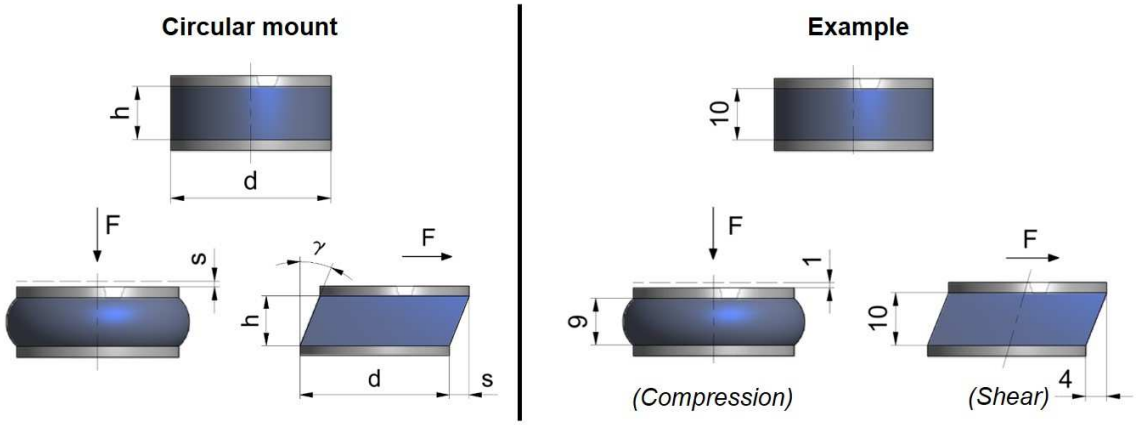

Figure 6: Circular mount and recommended nominal strain for compression and shear.

The compression stiffness correspondingly to Figure 6 can be calculated by:

$$k_\mathrm{c} = \frac{F}{s} \quad \text{with} \quad \sigma_\mathrm{c} = E_\mathrm{c}\varepsilon = \frac{F}{A} \quad , \quad \varepsilon = \frac{s}{h} \quad , \quad A = \frac{\pi}{4}d^2 \, . \tag{8}$$

Here E_c stands for the (compressive) Young's modulus and A for the cross sectional area perpendicular to the acting force F. For the stiffness finally follows:

$$k_c = \frac{\pi d^2 E_c}{4h} . \tag{9}$$

Here Young's modulus can be approximated by means of the form factor q as follows, [10]:

$$E_c = 3G(1 + q + q^2) \quad \text{with} \quad q = \frac{\pi d^2/4}{\pi dh} = \frac{d}{4h} . \tag{10}$$

The shear modulus can be empirically related to the Shore-A hardness, $H = 35 \ldots 75$ Sh-A, of rubber, [10]:

$$G = 0.086 \cdot 1.045^H . \tag{11}$$

Although rubber has a small shear modulus it is possible to considerably increase Young's modulus by means of geometry optimization, cf., Figure 7 (left).

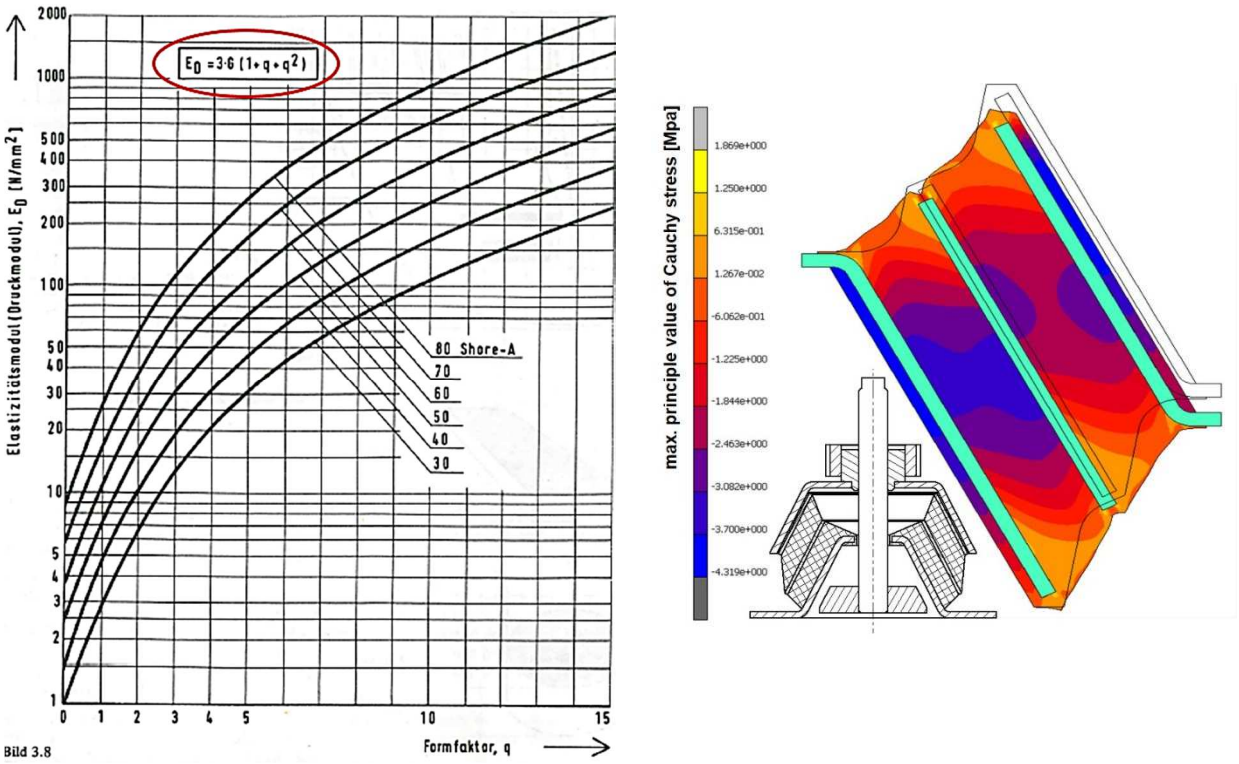

Figure 7: *Left:* Young's modulus as function of geometry, diagram borrowed from [10]. *Right:* FEA of the static load and the resulting stress profile within the rubber shape.

Shear loading and resulting deformations, cf. illustration in Figure 6 (right), can be investigated in a similar manner. For stiffness and shear stresses hold:

$$k_s = \frac{F}{s} \quad \text{and} \quad \tau = G \tan(\gamma) = \frac{F}{A} . \tag{12}$$

For small angular deflections Eq. $(12)_1$ and $(12)_2$ can be simplified to:

$$k_s = \frac{\pi d^2}{4h} G . \tag{13}$$

Shearing represents a volume-preserving deformation. Consequently effects from rubber incompressibility do not occur. Thus influences from geometry, represented by q, cannot be found in Eq. (13).

In many (more complex) geometries, e.g. conical mounts, shear and compressive loads occur parallel. Moreover, the above mathematical framework becomes much more complex. In such cases FEAs must be performed, which also allow to incorporate more complex materials behaviour, e.g. visco-elasticity.

2.2.1 Strength

After the quantification of stiffness the question about the maximal permitted deformation, $\varepsilon_{\max}$, of the RTM part occurs. Here the following thumb rule, which – surprisingly – holds for a wide range of geometries and dynamic applications, can be used, [11]:

Compression: $\varepsilon_{\text{nominal}} \leq 10 \ldots 15$ percent,
Shear: $\varepsilon_{\text{nominal}} \leq 40$ percent.

By using this rule it is possible to approximately apply 1 Mio loading cycles to the RTM components. Reducing $\varepsilon_{\text{nominal}}$ by factor 2 would increase possible loading cycles by factor 10 (e.g. $\varepsilon_{\text{nom, shear}} = 20$ percent $\Rightarrow$ 10 Mio loading cycles), et cetera. However, this thumb rule only holds for natural rubber with "moderate" ShA hardness and without any defects in the rubber-metal bonding layer.

Of course, uniaxial loading regimes are a hypothetical scenario. For many applications axial, lateral, torsional and cardanic loads occur, which can vary over time by amplitude and frequency. Such combined loads as well as complex geometries cannot be calculated by analytic thumb rules. Here FEAs are required, which allow – by means of appropriate materials law, e.g. Mooney-Rivlin or Neo-Hookean approach – to calculate stresses and strains within the rubber for different loading conditions.

Figure 7 (right) displays the FEA result for the rubber layers of a generator mount with the above mentioned target stiffness. Here we assumed the values presented at the end of Section 2.2 and write for the loads per mount:

$$F_{\text{m}} = \frac{\left(9.81\frac{\text{m}}{s^2}\cdot 15{,}000\ \text{kg}\right)}{4} = 37\ \text{KN} \quad \text{(load resulting from mass)},$$
$$M = \frac{P}{\omega} = \frac{3\ \text{MW}}{2\pi\cdot 1{,}500\ \text{rpm}} = 19\ \text{Nm} \quad \text{(torque)}. \tag{14}$$

Due to the 4-point mounting system and a lateral mount distance of 2000mm we obtain (with an assumed safety factor of $s = 2$) an additional dynamic load of 10 KN per mount. Consequently we have to consider for the vertical total loading per mount $F_{\text{total}} = 47$ KN.

A closer look at principle stresses allows us to evaluate mechanical durability. In particular a maximal tension stress value of $\max\{\sigma_1, \sigma_2, \sigma_3\} \leq +4$ MPa (max. principle value of Cauchy stresses) has established as an appropriate limit, which shows good agreement with experimental observations.

Beyond the investigation of loadings additional conditions have to be considered. There is a wide range of rubber compounds, natural and synthetic ones, available, which show different resistance during contact with environmental media. For example, possible interactions between rubber and ozone, mineral oils, salt water or cleaning agents have to be clarified. Furthermore peak and permanent temperature are important for choosing appropriate rubber compound. Finally, materials behavior like relaxation, creeping or heat expansion must be eventually quantified since these properties are stronger pronounced at rubber than for standard metals.

2.3 Fatigue Life of Rubber

In the following explanations we restrict ourselves to the question of rubber life-time due to oscillating loads. Aspects of rubber aging (following e. g. from chemical reactions between the rubber polymer network and environmental media, e. g. ozone) will not be considered; here we refer for example to [12].

In general rubber has a finite fatigue life – in particular under the presence of varying loads. The amount of possible loading cycles mainly depends on **(a)** the loading amplitude, **(b)** the characteristics of loading variation (swelling or oscillating loads) and **(c)** applied static preloads (mean loads). One possibility to quantify the amount of loading cycles under the presence of an existing, well-defined loading regime represents the Method of Woehler diagrams in combination with an appropriate damage accumulation theory (e. g. Palmgreen-Miner approach, [18]). This method is well-known from metals but shows in case of rubber various disadvantages. On the one hand side such diagrams must be experimental determined for each component design, which is a very time- and cost-intensive procedure. On the other hand – and this fact is more critical from the technical point-of-view – the approach cannot sufficiently consider different preload scenarios in a common diagram. Therefore so-called Smith-Haigh (S-M) diagrams are used in recent literature, e. g. [18,19], to investigate questions of rubber life-time. This method allows to investigate the above mentioned dependencies **(a)** - **(c)**. Moreover, the S-M diagrams are material-specific, i.e. they can be applied to different geometries, which contain same (or similar) rubber compound, e.g. NR with 50 Sh-A.

In order to quantify the above dependencies we introduce the following relations:

$$R = \frac{\sigma_{\min}}{\sigma_{\max}} \quad , \quad \hat{\sigma} = \frac{(\sigma_{\max} - \sigma_{\min})}{2} \quad , \quad \bar{\sigma} = \frac{(\sigma_{\max} + \sigma_{\min})}{2} \; . \tag{15}$$

It follows $R \geq 0$ for swelling loads and $R < 0$ for oscillating loads. Furthermore $\hat{\sigma}$ represents the oscillating amplitude and $\bar{\sigma}$ stands for the mean load.

It is worth-mentioning, that Eq. (15) only contains scalar quantities. However, realistic loading regimes would lead to a three-dimensional stress state within the rubber layer of the mountings. Consequently the question about an equivalent stress value occurs, which could reflect the 3D situation in an realistic manner. This question is an ongoing area of research and it seems that the appropriate equivalent stress depends on rubber geometry and loading case. Here we want to consider the maximum principal value of Cauchy Stress (as above), which is often used for investigations of rubber. By means of the loading scenario in Eq. (14) we obtain from the FEA: $\bar{\sigma} = 1.21$ MPa and $\hat{\sigma} = 0.7$ MPa.

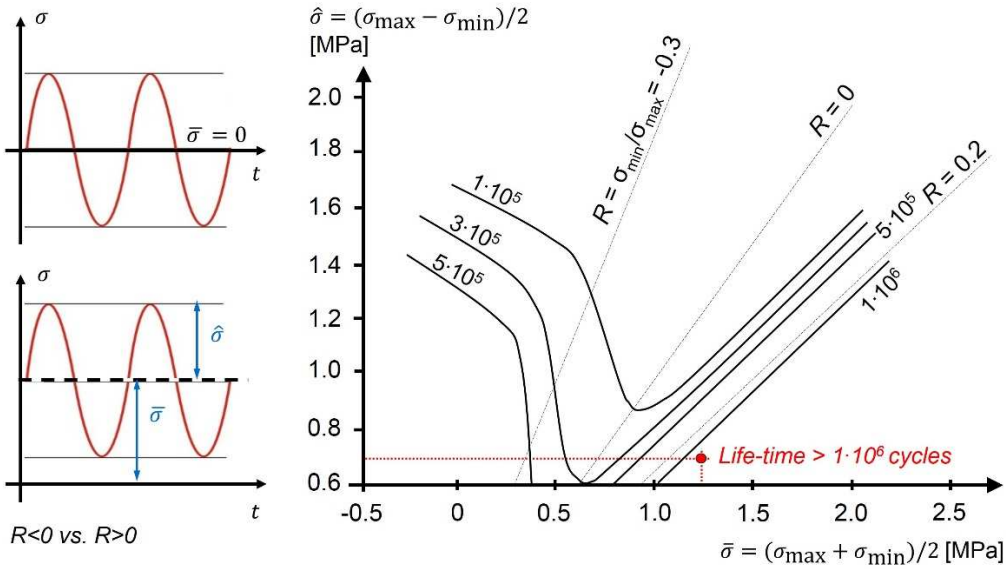

Figure 8: *Left*: Illustration of quantities in Eq. 15. *Right*: Smith-Haigh diagram for 50-NR rubber, borrowed from literature, cf., [19], and identification of the permitted loading cycles.

These values can be identified in the Smith-Haigh diagram as illustrated in Figure 8 (right). Obviously the line *R* = 0 defines, whether preloads have an advantageous or disadvantageous influence to the fatigue life. In the current case the expected life-time denotes more than $1 \cdot 10^6$ loading cycles.

3. Experimental tests of rubber components and mounting systems as part of an efficient development process

Because of the distinct nonlinear behavior of rubber materials, experimental investigations according to the rubber components itself as well as to the conditions while operating are still an important part of the development process of rubber components. Experimental investigations of the component yield necessary informations about the static and dynamic behavior of the component for different multi-physical loading cases whereas investigations of the overall system provide informations about the excitation, the dynamics and various interactions of adjoining structures and the resulting insulation rates. These informations are used for parameterization and validation of numerical simulation models, which are used during the design process as well as for validation of the overall insulation system.

3.1 Experimental analysis of rubber components

The analysis of stiffness and damping ratio is surely a widely-used experimental method of rubber components. Although it seems common, the execution as well as the interpretation of the results have to be carefully performed by the test field engineer. Moreover, the test procedure and the required experimental equipment have to be accurately chosen. Please note, the materials properties of rubber are highly nonlinear, change over time and depend on the loading history. Consequently constant values e. g. for stiffness

and damping ratio do not exist. Therefore all measurements represent a “snap-shot” and only allow for evaluations within a certain range.

Stiffness parameters can be determined for static and dynamic loadings, with and without preloads, for uniaxial or biaxial loads as well as for different ambient temperatures. Differences between these different scenarios can be significant. The static stiffness of rubber components is typically measured by hydraulic test rigs with single or multi-axis. To avoid parasitic errors the stiffness of the frame and load cell must be considerably higher w.r.t. the component stiffness. Moreover, for dynamic measurements any mechanical resonance cases of the frame and the sensing system must be outside of the investigated frequency range.

Dynamic stiffness and damping parameters are determined for different mono-frequent deflection amplitudes and varying frequencies. The resulting curves for stiffness and damping are functions of frequency, deformation amplitude, static preloads (in same or different directions) and sometimes even temperature. The interpretation can be done using FFT-methods as well as methods, which analyze the measured force-deflection hysteresis, cf. Section 2.1. The different approaches are defined in [13] and implemented in most modern test rigs for rubber components. However, FFT-methods are limited for linear systems and – consequently - the results of both methods significantly differ for rubber components with a pronounced non-linear behavior (for example for rubber with a high amount of filling materials, e.g. carbon black particles). Figure 9 (Left) shows the dynamic behavior of a generator mount with constant preload and varying deflection amplitudes. Here natural rubber were used with small amount of filler. Figure 9 (Right) displays the static deflection in vertical direction.

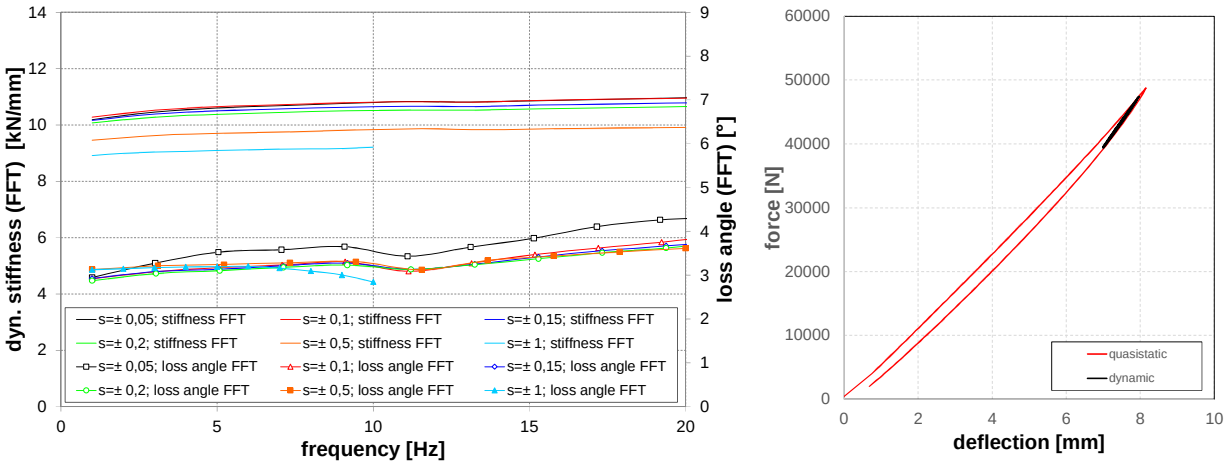

Figure 9: *Left:* dynamic behaviour of a heavy duty engine mount. *Right:* “quasi-static” deflection.

For amplitudes of 0.1 to 1.0 mm different curves of the dynamic stiffness occur whereas with increasing deflection amplitude the stiffness decreases. This phenomenon represents the so called “Payne-effect”, which was investigated first by the British rubber scientist A. R. Payne. Physically, the Payne effect can be attributed to deformation-induced changes in the material's microstructure, [14]. On the other hand the dynamic stiffness increases over frequency, whereas the loss angle - in contrast to viscous damping elements - is approximately constant.

Results of the above mentioned analysis are used to parameterize simulation models and analytical design methods which are widely used for the design of insulation systems. Such methods yield reliable results in a frequency range up to approximately 100 Hz.

To investigate the acoustic behavior of elastic, rubber-based components other analysis methods must be applied. Here the Transmission Loss (TL) and the Insertion Loss (IL) are two physical values, which describe the acoustic behavior of isolators. Typically they are used to characterize rubber components in a frequency range of 0.1 kHz to 2 kHz. The transmission loss is often measured on special NVH test rigs for rubber specimen and smaller components, which use electro-dynamic shakers to realize high excitation frequencies of up to 2 kHz. The measurement of the insertion loss is typically performed in field in order to compare different isolators. For the calculation of TL and IL the isolator can be described by a mechanical four pole, [15]:

$$\begin{bmatrix} F_1 \\ v_1 \end{bmatrix} = \underline{A} \cdot \begin{bmatrix} F_2 \\ v_2 \end{bmatrix} = \begin{bmatrix} a_{11} & a_{12} \\ a_{21} & a_{22} \end{bmatrix} \cdot \begin{bmatrix} F_2 \\ v_2 \end{bmatrix}. \tag{16}$$

The transmission loss can then be calculated in two ways, first (see Eq. 16) as TL of the velocities on the excitation side (index 1) and isolation side (index 2)

$$TL_v = \frac{v_1}{v_2} = a_{22} + a_{21}\frac{F_2}{v_2} = a_{22} + a_{21}Z_2 \tag{17}$$

and, second, as TL of the affecting forces at both sides

$$TL_F = \frac{F_1}{F_2} = a_{11} + a_{12}\frac{v_2}{F_2} = a_{22} + \frac{a_{12}}{Z_2}\,. \tag{18}$$

The transmission loss of rubber components can be analyzed by measuring the accelerations or forces directly at the isolator joints. The insertion loss IL is defined by:

$$IL = \frac{F_2}{F_2'} = \frac{v_2}{v_2'} = \frac{a_{22}'Z_1 + a_{21}'Z_1Z_2 + a_{12}' + a_{11}'Z_2}{a_{22}Z_2 + a_{21}Z_1Z_2 + a_{12} + a_{11}Z_2}\,. \tag{19}$$

Both values, TL and IL, depend on the dynamic behavior of the adjoining structures. These dynamics can be described by the mechanical impedance $Z = \frac{F}{v}$. Obviously TL_F and TL_v only depend on the impedance Z_2 of the isolation side, whereas the insertion loss IL also depends on the source impedance Z_1. Therefore a comparison of different components only holds for analyses with identical adjoining structures.

If the different impedances are known, the quantities TL and IL could be expressed in an analytical way. Figure 10 (left, solid line) illustrates simulation results of the transmission loss for a typical single mass spring damper system with ideal spring and without mass and geometry effects.

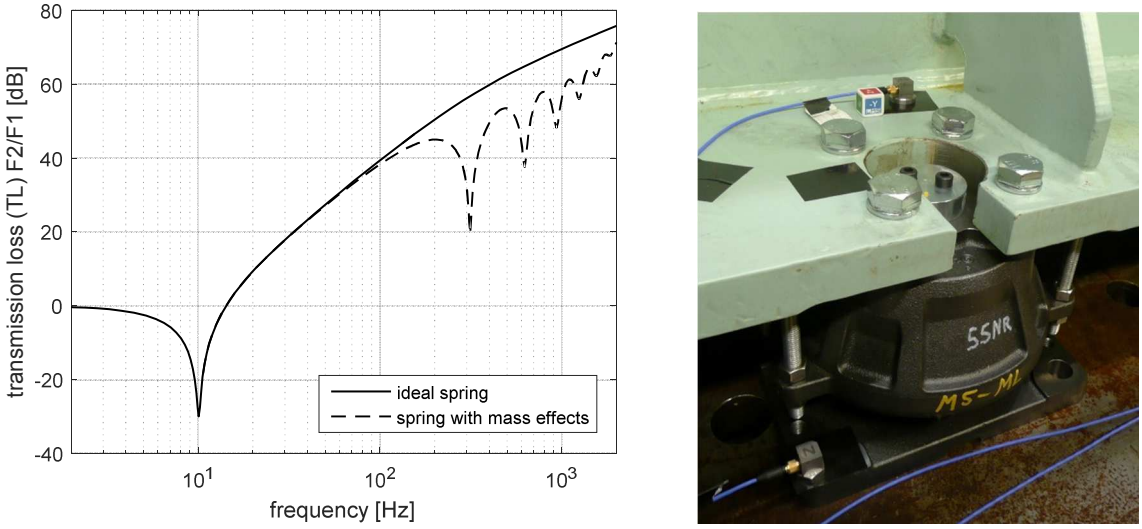

Figure 10: *Left*: Transmission loss of a single mass spring damper system excited by force (simulation). *Right*: on-site measurements of generator mountings.

The dashed line shows the simulation of a mass effected spring. For frequencies up to ca. 100 Hz mass effects from the inner spring can be neglected. For higher frequencies these effects lead to a sequential decline of the transmission loss, which are most distinctive for rubber mounts with intermediate layers.

3.2 Experimental analysis of operation conditions

In addition to the experimental analysis of rubber components in laboratory on-site measurements of the overall vibration system under typical operation conditions (or with synthetic excitation) are very useful to benchmark the mounting system. Such analyses would provide a detailed understanding of sources and consequences of operational vibrations.

Methods for such on-site investigations are: **(i)** measurement of the IL of mounting systems (see above), **(ii)** analysis of vibration velocities specified in DIN ISO 10816, cf. [16], **(iii)** order analysis of rotary machineries done for different operation scenarios like run ups and run downs, **(iv)** Wavelet-analysis performed for steady state operation as well as for transient scenarios like machinery shut downs, **(v)** analysis of operational deflection shapes in order to obtain informations about system- and structure reactions for different load cases and **(vi)** operational or experimental modal analyses to identify natural frequencies and –modes of the dynamic system [17].

Figure 11 shows test results of an order analysis for a 4.5 MW power unit (PU) mounted with heavy duty generator mounts (see Figure 10, right). Such PU is typically used for stationary power generation and

differ from the aggregates used in wind energy turbines. However, the results allows to exemplarily illustrate, which information can be obtained from the vibration system. The PU consists of a synchronous generator with five terminal pairs, which is powered by a nine-cylinder diesel engine. Both units are coupled by a flexible clutch and mounted on a base frame. Figure 10 (lower panel) illustrates the physical structure of the PU.

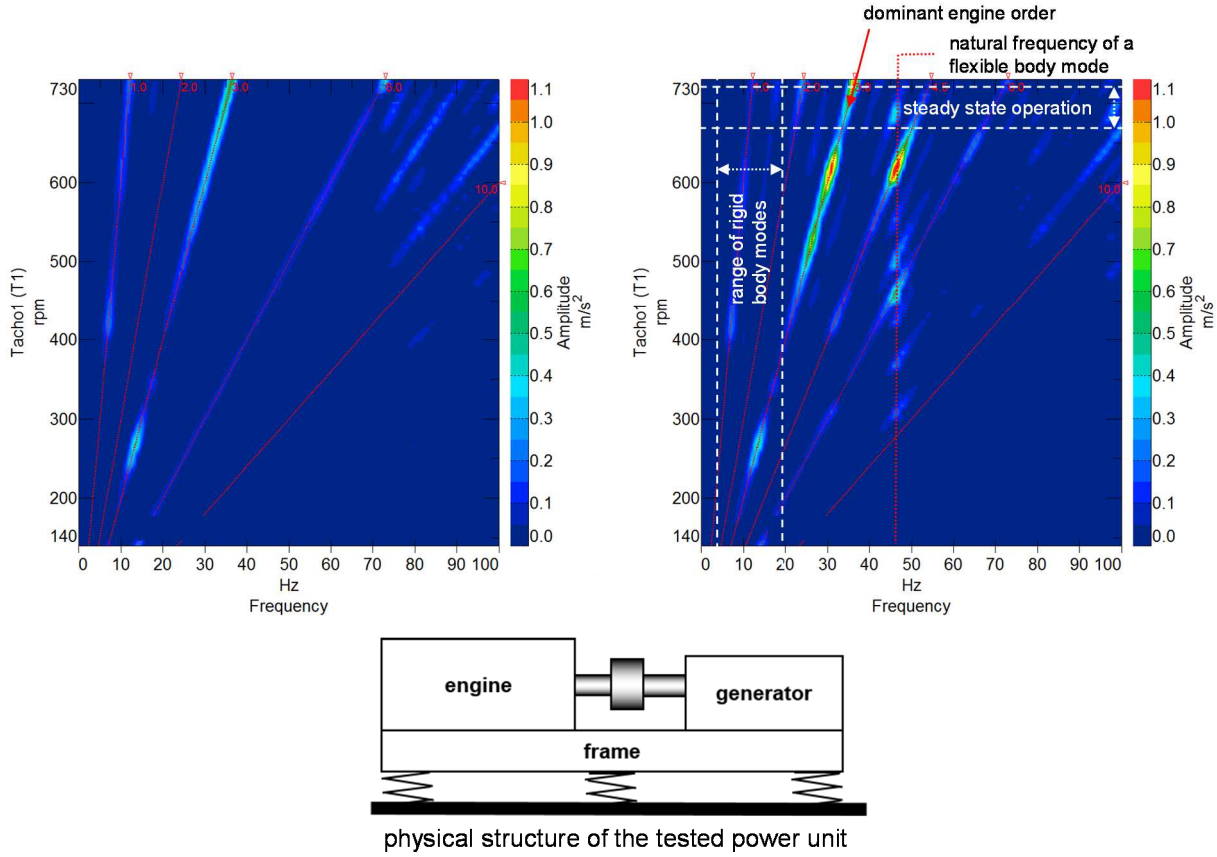

Figure 11: Campbell-plot: acceleration levels for PU – break down. *Left:* mount engine side – vertical direction. *Right:* mount, generator side – vertical direction.

From the Campbell-plots in Figure 11 one can see: **(a)** the first order excited by unbalanced masses; **(b)** the third order excited by forces of the combustion process of the engine and **(c)** the 10th order coming from forces due to nonlinearities of the magnetic field of the generator. Furthermore you can find the frequency range, in which the rigid body modes of the PU are located. From the engineering point-of-view the best mounting system design is obtained, if the frequencies of the rigid body modes are located below the frequency range of steady state operation and doesn't overlap with it. Thus, good insulation of the adjoining structures as well as low amplitudes at the oscillator side can be achieved.

Conclusion

In the present contribution different aspects of rubber-based elastic mounts were illustrated. Such mounts are widely used in windmills in order to decouple structure born noise, to insulate sensible components w.r.t. shocks or to minimize constraint forces in the power train.

After a brief introduction into the necessity of different mountings along the power train we turned the attention to the stepwise development process of RTM parts. Various aspects of vibration dynamics, rubber strength calculations and fatigue life estimations were explained. For this reason a conical mount geometry, which is typically found for mounting windmill generators, were used and exemplarily calculated. The article ends with a brief illustration of experimental methods in order to investigate and evaluate mounting systems in the real vibration system with adjoining structures.

The article provides a guideline, that could help design engineers during the development process of rubber based components taking into account questions of insulation, damping, rubber strength and fatigue life.

Acknowledgement

The authors gratefully acknowledge the colleagues D. Gürtler and R. Mischke for their support during preparation of various illustrated data.

References

[1]. DIN 740-2:1986-08. „Antriebstechnik; Nachgiebige Wellenkupplungen; Begriffe und Berechnungsgrundlagen“. Beuth Verlag: Berlin, 1986.

[2]. Kunze, H. “Aktiver Tilger - Unterdrückung von tonalen Komponenten bei Windenergieanlagen”. 5th Rheiner Windenergie-Forum, 2009: 1-29.

[3]. Mitsch, F. „Elastomerlagerung mit regulierbarer Steifigkeit“. Europäische Patentschrift EP 1 566 543 B1, August 26, 2009.

[4]. Wahl T., Biedermann T., Epe C., Heinze R., Kameier F. „Ist Lärmschutz bei Windenergieanlagen notwendig?“. DAGA 2014 – 40. Deutsche Jahrestagung für Akustik, Oldenburg, 2014: 210-211.

[5]. Mitschke M., Wallentowitz H. “Dynamik der Kraftfahrzeuge” 4. Auflage. Springer: Berlin Heidelberg New York, 2004: 257-264.

[6]. VDI Richtlinien VDI 3830 Part 5. “Damping of materials and members – Experimental techniques for the determination of damping coefficients”. Verein Deutscher Ingenieure: Düsseldorf, 2005.

[7]. Müller W.H., Ferber F. “Technische Mechanik für Ingenieure” 2. verbesserte Auflage. Fachbuchverlag Leipzig im Carl Hanser Verlag: München Wien, 2005: 285-291.

[8]. Waas G. “Dämpfung von Bauwerksschwingungen”. *Dämpfung, Duktilität, Nichtlineares Bauwerksverhalten*; Vortragsband der 4. Jahrestagung der Dt. Gesellschaft für Erdbeben-Ingenieurwesen und Baudynamik, Hrsg. H-J Dolling, 1989; 1-30.

[9]. Hau E. „*Windkraftanlagen*“ 5. Auflage. Springer-Vieweg: Berlin Heidelberg New York, 2014: 252-278.

[10]. Battermann W., Köhler R. „*Elastomere Federung, Elastische Lagerungen*“. Verlag von Wilhelm Ernst und Sohn: Berlin München, 1982: 52-63.

[11]. Beitz W., Küttner K.-H. ”*Dubbel – Taschenbuch für den Maschinenbau*” 16. Auflage. Springer Verlag: Berlin Heidelberg New York, 1987: G57.

[12]. Spreckels J. „Ein Beitrag zur Berücksichtigung von Alterungs- und Umwelteinflüssen bei der Lebensdauerprüfung von Elastomerbauteilen“, Dissertation, VDI Verlag, Düsseldorf: 2013.

[13]. DIN EN ISO 10846-1-3:1998. “Acoustics and vibration - Laboratory measurement of vibro-acoustic transfer properties of resilient elements”. Beuth Verlag: Berlin, 1998.

[14]. Gent A. N. “*Engineering with Rubber: How to Design Rubber Components*” 3rd Edition. Hanser Verlag, München: 2012.

[15]. TrelleborgVibracoustic (Hrsg.) “*Schwingungstechnik im Automobil*”. Verlag Vogel Business Media: 2014.

[16]. DIN ISO 10816-1:2013. “Mechanical vibration - Evaluation of machine vibration by measurements on non-rotating parts”. Beuth Verlag: Berlin, 2013.

[17]. Zeller P. “*Handbuch Fahrzeugakustik*” 2. Auflage. ATZ/MTZ Fachbuch, 2012.

[18]. Spitz M. „Modellbasierte Lebensdauerprognose für dynamisch beanspruchte Elastomerbauteile“, Dissertation, Fakultät für Ingenieurwissenschaften, Universität Duisburg-Essen, 2012.

[19]. André N. “Critére local d’amorage de fissures en fatigue dans un élastomére de type nr.” Thése Ecole Nationale Supérieure des Mines de Paris, 1997.